Seasonal Variability of the Carbonate System and Air–Sea CO_2 Flux in the Outer Changjiang Estuary, East China Sea

Jing Liu[1], Richard G. J. Bellerby[1,2]*, Xiaoshuang Li[1] and Anqiang Yang[1]

[1] State Key Laboratory of Estuarine and Coastal Research, East China Normal University, Shanghai, China, [2] Norwegian Institute for Water Research, Bergen, Norway

Three field surveys were conducted in the outer Changjiang Estuary on the inner shelf of the East China Sea in March, July, and October, 2018. Observations of total-scale pH (pH_T), total alkalinity (A_T), and calculated total dissolved inorganic carbon (C_T), the partial pressure of CO_2 (pCO_2), and the air–sea CO_2 exchange flux (FCO_2) were studied in the surface waters. The results showed that the Changjiang Diluted Water (CDW) area was a source of atmospheric CO_2 in July and October (4.97 and 8.67 mmol CO_2/m^2/day, respectively). The oversaturation of CO_2 was mainly ascribed to the respiration of terrestrial organic and inorganic materials sourced from the Changjiang River discharge, overwhelming the CO_2 uptake due to primary productivity despite the high phytoplankton biomass in summer. The air–sea CO_2 flux was greater in October than in July in the CDW, which is attributed to the increasing wind speed. In contrast, the Yellow Sea Water (YSW) and the East China Sea Shelf Water (ECSSW) were a weak CO_2 sink in March (–0.71 and –2.86 mmol CO_2/m^2/day, respectively) and July (–1.28 mmol CO_2/m^2/day in the ECSSW) following the CO_2 uptake of phytoplankton production, however, they were a CO_2 source by October (3.30 mmol CO_2/m^2/day in the YSW and 1.18 mmol CO_2/m^2/day in the ECSSW). The cooling effect during the cold season reduced the sea surface pCO_2, resulting in a CO_2 sink in the CDW, YSW, and ECSSW areas in March. However, the regions became a source of atmospheric CO_2 in October, possibly driven by vertical mixing, which brought C_T-enriched bottom water to the surface and increased the pCO_2. The study region was a net CO_2 sink in March and a net CO_2 source in July and October with an average FCO_2 of –1.25, 1.71, and 3.06 mmol CO_2/m^2/day, respectively.

Keywords: carbon dioxide, water masses, air–sea CO_2 exchange, seasonal variability, Changjiang Estuary, East China Sea

INTRODUCTION

Although coastal systems contribute only a small percentage of the global ocean surface area (a little over 7%), they play a disproportionately important role in the global carbon cycle and ultimately affect global climate change processes (Chen et al., 2013). The annual mean for the net CO_2 uptake by the global ocean is estimated to be –2.5 ± 0.6 GtC/year (Friedlingstein et al., 2019), in

which marginal seas absorb approximately 8–18% of CO_2 (0.2–0.45 GtC/year) (Borges et al., 2005; Laruelle et al., 2010; Cai, 2011). Coastal margins are the most heterogeneous areas of the oceans in the world, with strongly contrasting physical and biogeochemical activity (Cai and Dai, 2004; Borges et al., 2005). The air–sea CO_2 flux ($F\mathrm{CO_2}$) in global marginal seas is still a matter of debate, although field surveys and models show that they generally act as a net atmospheric CO_2 sink (Chen and Borges, 2009; Bauer et al., 2013).

Coastal systems can be classified into two distinct physical–biogeochemical groups: ocean-dominated margins (OceMars) (Dai et al., 2013); and river-dominated ocean margins (RioMars) (McKee et al., 2004). OceMars exchanges with the open ocean through the horizontal intrusion of water masses, vertical mixing, and upwelling. Their CO_2 sink/source status mainly depends on the balance between C_T/nutrients imported from the open ocean and the subsequent biological consumption in the euphotic zone (Dai et al., 2013). However, RioMars are greatly affected by significant riverine inputs of dissolved and particulate terrestrial material (McKee et al., 2004). Generally, they act as a CO_2 sink at high river discharges, because the CO_2 consumed by biological production exceeds the CO_2 produced by the decomposition of terrestrial organic matter (Cao et al., 2011; Tseng et al., 2011; Guo et al., 2012).

The East China Sea (ECS) is one of the broadest marginal seas in the world and is characterized by high biological production. Since the 1990s, the carbonate dynamics of the ECS have been extensively studied, and indications are that it is a net CO_2 sink (Tsunogai et al., 1997, 1999; Shim et al., 2007; Chou et al., 2009, 2011, 2013; Guo et al., 2015). The ECS shelf may absorb as much as 0.013–0.030 GtC/year (Wang et al., 2000). Due to the high Changjiang River discharge, the ECS is a typical river-dominated coastal system in summer, where it acts as a net CO_2 sink (Chou et al., 2017). However, the ECS has seasonal and spatial variations in CO_2 flux and is a moderate or large net atmospheric CO_2 sink throughout the year, except in autumn (Shim et al., 2007; Zhai and Dai, 2009). The Changjiang Diluted Water (CDW) is confined to an area off the Changjiang Estuary and is a CO_2 source, while the East China Sea Shelf Water (ECSSW) was a CO_2 sink both in spring and summer (Qu et al., 2017). However, estimates of the $F\mathrm{CO_2}$ in the inner shelf region of the ECS are based on limited data (e.g., Tan et al., 2004; Zhai and Dai, 2009). The region has undergone significant anthropogenic environmental change, such as eutrophication and acidification (Wang, 2006; Zhu et al., 2011). Therefore, an improved spatial and temporal understanding of the ECS inner-shelf carbon chemistry is needed to further improve the accuracy of $F\mathrm{CO_2}$.

In this study, the carbonate dynamics and $F\mathrm{CO_2}$ of the outer Changjiang estuary were investigated in spring, summer, and autumn based on three field surveys conducted in 2018. We first describe the seasonal surface spatial distributions of carbonate parameters, total-scale pH (pH_T), total alkalinity (A_T), total dissolved inorganic carbon (C_T), the surface partial pressure of CO_2 ($p\mathrm{CO_2}$), and their relationships with various water masses in different seasons. Then, we calculated $F\mathrm{CO_2}$ for various water types, compared the seasonal changes in air–sea CO_2

fluxes, and discussed controls. Finally, based on our study and previously published results, we summarized the knowledge of CO_2 fluxes in the outer Changjiang estuary and provided a baseline for assessing future changes in the regional oceanic carbonate system.
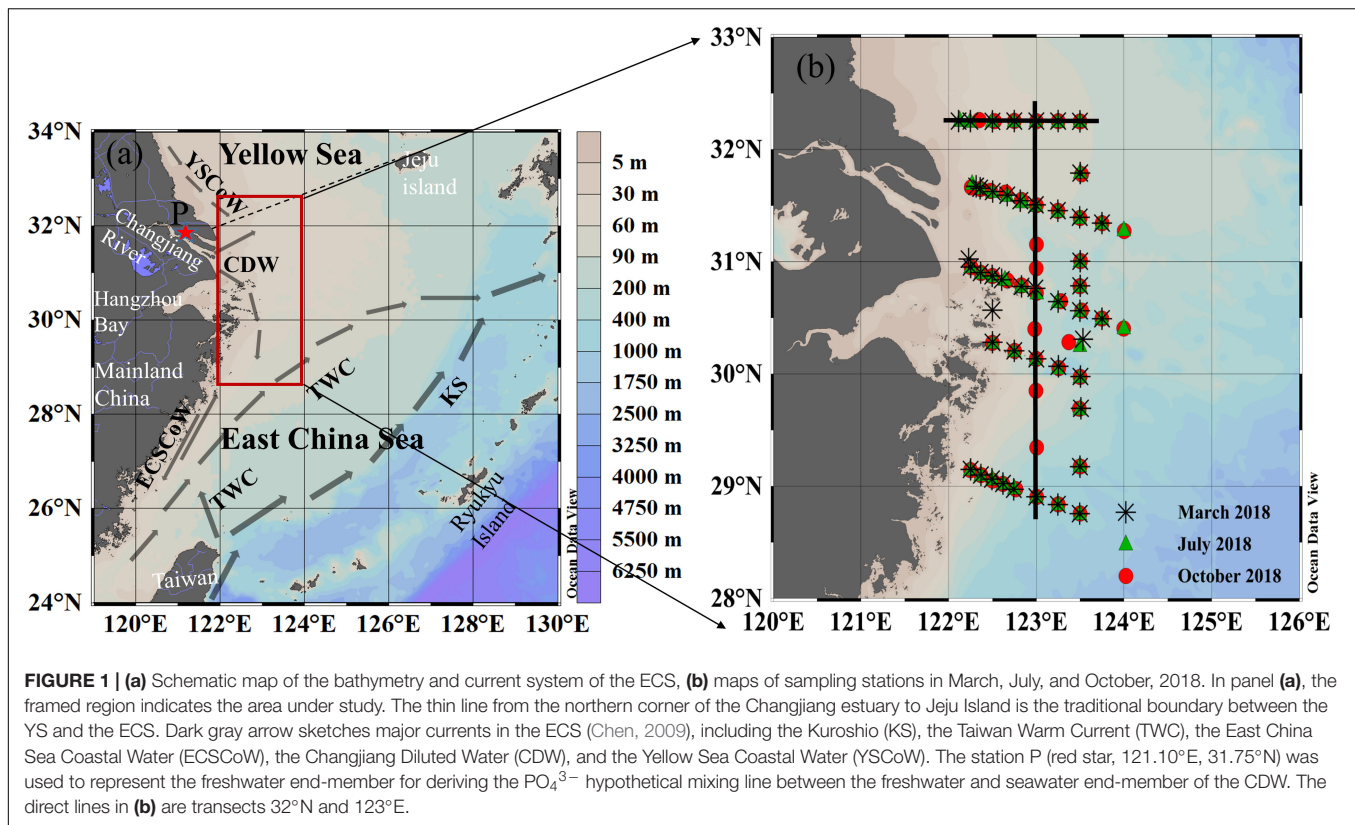
MATERIALS AND METHODS

Study Sites

The ECS in the Western Pacific receives a massive runoff annually from the Changjiang River, making it one of the largest marginal seas (Chou et al., 2009). A line running northeastward from the Qidong Cape to Jeju Island is operationally the northern boundary of the ECS. The southeast boundary is the Ryukyu Islands, the southern boundary is Taiwan, and the western boundary is mainland China (Qu et al., 2015). The annual Changjiang River discharge at the Datong gauging station was 896 km^3 during 1950–2010 (Luan et al., 2016), with the highest monthly discharge (July) being approximately 5-6 times higher than the lowest discharge occurring in January (Dai and Trenberth, 2002). A high amount of nutrients and terrestrial material along with freshwater are transported to the ECS, which influence the seasonal and spatial variability of hydrological and biogeochemical properties.

The study region covers a 4° × 2° area from 128.5 to 32.5°N and from 122 to 124°E (the rectangle in **Figure 1a**), located in the outer Changjiang estuary of the ECS. Its western part is mainly affected by the Changjiang River discharge, where high $p\mathrm{CO_2}$ freshwater meets the highly productive ECSSW (Zhai et al., 2007; Yu et al., 2013). The CDW is formed by the mixing of the Changjiang River discharge and shelf seawater; and is characterized by high nutrient content and low salinity (Gong et al., 1996). As the northeast East-Asian monsoon occurs from October to April, switching to the southwest monsoon from May to July (Zhai et al., 2014a,b), the CDW flows northeastward and extends toward Jeju Island, reaching the southeastern Yellow Sea (YS) in summer and southward along the coast of Zhejiang–Fujian through the Taiwan Strait in winter (Chang and Isobe, 2003; Chen, 2009). The northern part of the study area is usually affected by Yellow Sea Water (YSW), characterized by intermediate salinity, low temperature, and low nutrients (Gong et al., 1996). In summer, the YSW is contained in the YS because of the strong northeastward expansion of CDW (Chen, 2009; Qi et al., 2014). The ECSSW is mainly found over the central continental shelf between the CDW and Kuroshio (KS) (Qi et al., 2014), a high temperature and salinity water mass resulting from the mixing of coastal and offshore water.

Sampling and Analytical Methods

The field investigations were carried out aboard the R/V *Kexue 3* from March 9 to 19, July 11 to 20, and October 11 to 22, 2018. The sampling stations and cruise transects are shown in **Figure 1b**. The sampling and analytical methods for carbonate parameters strictly followed the recommended standard operating procedures described by Dickson et al. (2007) and the methods of Zhai et al. (2014a,b). For each station, water

FIGURE 1 | (a) Schematic map of the bathymetry and current system of the ECS, **(b)** maps of sampling stations in March, July, and October, 2018. In panel **(a)**, the framed region indicates the area under study. The thin line from the northern corner of the Changjiang estuary to Jeju Island is the traditional boundary between the YS and the ECS. Dark gray arrow sketches major currents in the ECS (Chen, 2009), including the Kuroshio (KS), the Taiwan Warm Current (TWC), the East China Sea Coastal Water (ECSCoW), the Changjiang Diluted Water (CDW), and the Yellow Sea Coastal Water (YSCoW). The station P (red star, 121.10°E, 31.75°N) was used to represent the freshwater end-member for deriving the PO_4^{3-} hypothetical mixing line between the freshwater and seawater end-member of the CDW. The direct lines in **(b)** are transects 32°N and 123°E.

samples were collected at two or three depths using 12 L Niskin bottles mounted on a rosette assembly. Temperature and salinity were measured using a conductivity–temperature–depth (CTD) system (SBE 9/11-plus).

Samples of nutrients were first filtered with a 0.45 μm Whatman GF/F membrane and then stored in 250 mL high-density polyethylene (HDPE) bottles and stored at –20°C until chemical analysis. Nitrate (N), phosphate (PO_4^{3-}), and silicate (Si) were determined using a segmented flow analyzer (model: Skalar SANPLUS, Netherlands) with a precision <5% (Zhang et al., 2007); the detection limits were 0.14 μM for N, 0.06 μM for PO_4^{3-}, and 0.07 μM for Si.

The Chlorophyll a (Chl a) samples were collected 250 mL from Niskin bottles, first filtered through 300 μm meshes followed by 0.68 μm Whatman GF/F membranes, which were then folded rapidly within an aluminum foil and stored at –20 °C until analysis. Chl a on membranes was extracted using 90% acetone and then analyzed using a fluorescence spectrophotometer (Lengguang Tech F9700) based on the procedure described by Parsons et al. (1984).

A_T samples were stored in 250 mL HDPE bottles without filtering. The samples were poisoned with 100 μL saturated mercuric chloride ($HgCl_2$) solution and stored in a laboratory at 25°C. A_T was determined at 25°C by versatile instruments for the determination of titration alkalinity (VINDTA 3C) (Mintrop et al., 2000). Certified reference materials (CRM; Batch 156) from A. G. Dickson's lab at the Scripps Institute of Oceanography were used for calibration and accuracy assessments of A_T

measurements, and the accuracy and precision were determined to be higher than ± 2 μmol/kg.

Samples for pH_T were stored in 500 mL high-quality borosilicate glass bottles without filtering, poisoned with 200 μL saturated $HgCl_2$ solution, and stored at room temperature until measurement in the laboratory. pH_T was measured using an automated flow-through system for embedded spectrophotometry (Reggiani et al., 2016) with a precision of ±0.0005 pH unit. The indicator dye used was thymol blue (TB) sodium salt (TCI #FCP01, Tokyo Chemical Industry). Although Hudson-Heck and Byrne (2019) stated that "only low levels of impurities are typically present in off-the-shelf TB," we evaluated the impurity of the indicator used following the approaches of Douglas and Byrne (2017) and Hudson-Heck and Byrne (2019) and identified that the pH_T correction was –0.00083. We measured the pH_T of CRM during the process of measuring the pH_T samples as a standard procedure. We calculated the CRM reference pH_T value at a temperature of 25°C using CO2SYS based on the salinity (33.455), C_T, A_T, PO_4^{3-}, and Si of CRM batch 156. The dissociation constants for H_2CO_3 were determined by Lueker et al. (2000), and the dissociation constant for HSO_4^- ions was determined by Dickson (1990). We measured the pH_T value of CRM at 25°C and salinity of 33.455 and compared it with the CRM reference pH_T (**Supplementary Figure 1**). The mean and standard deviation (SD) of the comparison were 0.0012 ± 0.0036 ($n = 44$) and 93% of residuals were within ± 0.006.

Calculation of Other Carbonate System Parameters

Total dissolved inorganic carbon (C_T) and pCO_2 were calculated using *in situ* temperature, salinity, PO_4^{3-}, Si, measured pH_T, and A_T using the CO2SYS.XLS (version 16) program developed by Pelletier et al. (2011), which is an updated version of CO2SYS.EXE (Lewis and Wallace, 1998). The dissociation constants for H_2CO_3 were determined by Lueker et al. (2000), and the dissociation constant for HSO_4^- ions was determined by Dickson (1990). In this study, we compared the carbonate properties obtained from the constants of Hansson (1973), Mehrbach et al. (1973), Dickson and Millero (1987), Lueker et al. (2000) and Millero et al. (2006) constants. We then found that, for our data range of temperature, salinity, pH_T, and A_T, the calculated pCO_2 difference was ~3%. However, the carbonate parameters were calculated following Lueker et al. (2000) as recommended for best practices (Dickson et al., 2007). Thus, we chose the one for our calculations. Based on our measurements, uncertainties in pH_T and A_T measurements resulted in a calculated uncertainty of approximately ± 2 μatm in pCO_2.

CO_2 Flux Calculations

FCO_2 (mmol CO_2/m^2/day) was calculated from:

$$FCO_2 = k \times s \times \triangle pCO_2 \qquad (1)$$

where k is the CO_2 transfer velocity (cm/h), s is the solubility of CO_2 in seawater (mol/kg) (Weiss, 1974), and $\triangle pCO_2$ is the difference between the sea surface pCO_2 and the CO_2 concentration in the atmosphere. Atmospheric CO_2 concentrations were derived from the Tae-ahn Peninsula observation site (36.7376°N, 126.1328°E; Republic of Korea[1]), after correction for water vapor pressure to 100% humidity with *in situ* temperature and salinity data (Weiss and Price, 1980). A positive flux indicates the release of CO_2 from the ocean to the atmosphere. The gas transfer velocity is a function of wind speed. However, as there is currently no universally accepted relationship, we compared the relationships between k and wind speed proposed by Nightingale et al. (2000) (hereafter referred to as N00), Ho et al. (2006) (H06), and Wanninkhof et al. (2009) (W09) to estimate FCO_2 in this study. The reason is that the N00 and H06 used the dual-deliberate tracer methods of ^{3}He and SF_6 to obtain direct estimates of k, and the experiments by N00 were performed in coastal seas, while the latter was performed in the Southern Ocean. However, W09 proposed using the nonzero intercepts for accounting for zero wind speed gust environments or zero wind-driven processes and utilizing the global bomb ^{14}C constraint and information from the literature to determine k.

$$N00 \qquad k = \left(0.333 \times u + 0.222 \times u^2\right) \times (Sc/660)^{-0.5} \qquad (2)$$

$$H06 \qquad k = 0.266 \times u^2 \times (Sc/660)^{-0.5} \qquad (3)$$

$$W09 \qquad k = \left(3 + 0.1 \times u + 0.064 \times u^2 + 0.011 \times u^3\right)$$
$$\times (Sc/660)^{-0.5} \qquad (4)$$

[1]http://www.esrl.noaa.gov/gmd/dv/site

where u is the daily wind speed at a height of 10 m (in m/s). We used the daily average wind speed from CCMP Version–2.1 analyses produced by Remote Sensing Systems with a spatial resolution of 0.25° × 0.25° grids.[2] Sc is the Schmidt number for CO_2 in seawater computed from *in situ* temperature data (Wanninkhof, 2014).
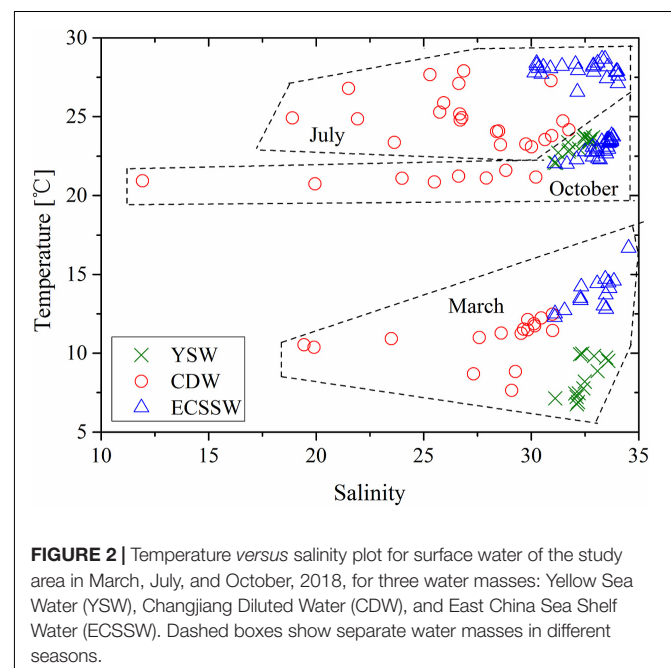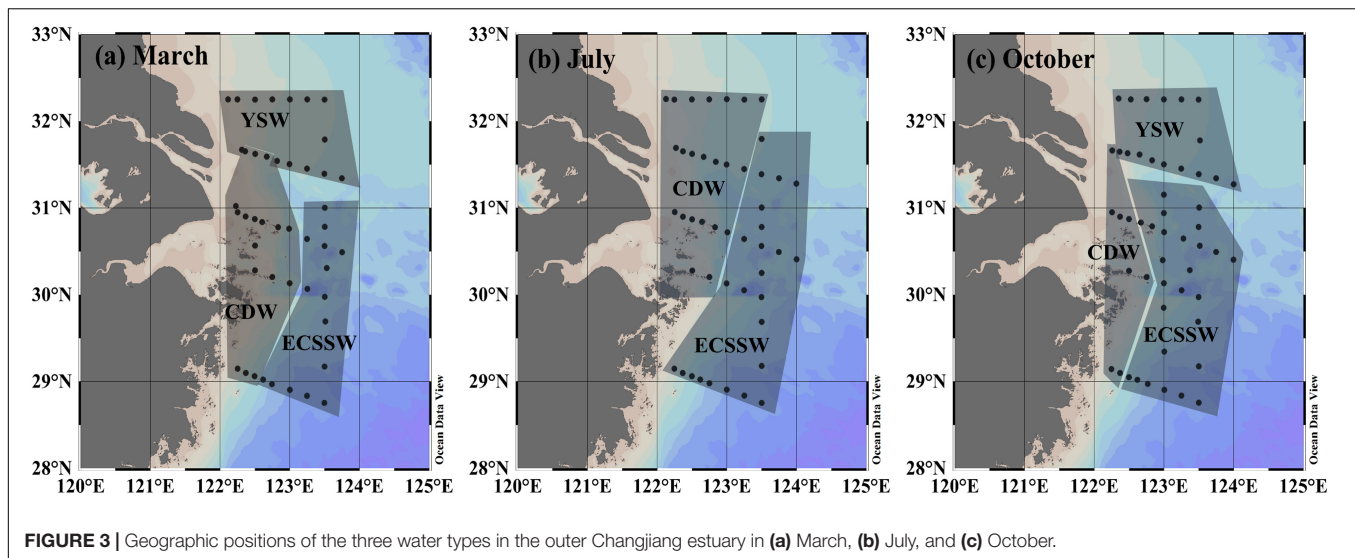
RESULTS

Classification of Water Types

In our study, the surface waters were grouped into three types, namely, (1) YSW, (2) CDW, and (3) ECSSW, according to the classification described by Chou et al. (2009), Qi et al. (2014), and Zhai et al. (2014a) (T–S diagram, **Figure 2**). The temperature and salinity variations of the three water types are listed in **Supplementary Table 1**. The locations of the various water types in the three surveys (**Figure 3**) were generally consistent with the known distribution pattern in the ECS (**Figure 1a**). The YSW was classified under the northeast part of our study area in March and October, whereas the CDW was identified outside the Changjiang River estuary, where the water depth was <50 m. The remaining area was identified as ECSSW (**Figure 3**).

Distribution of Hydrological and Carbonate Parameters in Various Water Types

The surface distributions of temperature, salinity, pH_T, A_T, C_T, and pCO_2 in March, July, and October are presented in **Supplementary Figure 2**. Their range, average, and SD

[2]http://www.remss.com/measurements/ccmp/

FIGURE 2 | Temperature *versus* salinity plot for surface water of the study area in March, July, and October, 2018, for three water masses: Yellow Sea Water (YSW), Changjiang Diluted Water (CDW), and East China Sea Shelf Water (ECSSW). Dashed boxes show separate water masses in different seasons.

FIGURE 3 | Geographic positions of the three water types in the outer Changjiang estuary in **(a)** March, **(b)** July, and **(c)** October.

values for the three different water types are summarized in **Supplementary Table 1**. The distributions of these parameters not only have significant seasonal variations but also vary between different water masses.

The distributions of temperature and salinity are consistent with the circulation systems and hydrological environments of the ECS (Lee and Chao, 2003). In our three surveys, the intermediate salinity (31.11–33.57 in March and 31.08–32.87 in October) was limited in the YSW, while higher temperatures and salinity (12.28–16.67°C and 31.09–34.52; 26.56–28.66°C and 30.15–34.04; 22.00–23.81°C and 31.09–33.80 in March, July, and October, respectively) were observed in the ECSSW as a result of the high temperature and salinity of the Taiwan Warm Current (TWC). Low salinities (< 31) occurred in the CDW (19.44–31.00, 18.89–31.75, and 11.93–30.22 in March, July, and October, respectively) with low temperatures in July (23.08–27.90°C) and October (20.74–21.60°C) (**Supplementary Figures 2A,B**).

Generally, the CDW had the lowest pH_T (pH_T < 8). Intermediate pH_T values were mainly detected in the YSW area (8.042–8.104 in March and 7.927–8.008 in October), while a relatively high pH_T was found in the ECSSW area (8.078–8.117 in March and 7.938–8.085 in October). However, in summer, the highest pH_T (8.420) and the lowest pH_T (7.729) values occurred in the CDW area, the highest value may be the result of net biological production, and the lowest was due to biological respiration and the decomposition of organic matter (**Supplementary Figure 2C**).

Similar to the distribution of pH_T, low A_T values always occurred in the CDW (2168–2317, 2069–2232, and 1982–2281 µmol kg^{-1} in March, July, and October, respectively). In March and October, a high A_T was found in the YSW (2263–2356 and 2227–2282 µmol/kg in March and October, respectively), while the ECSSW had intermediate A_T values (2246–2273 and 2229–2248 µmol/kg in March and October, respectively) (**Supplementary Figure 2D**). The high A_T in YSW may result from Huanghe River discharge with high A_T concentrations (2874–3665 µmol/kg) (Chen et al., 2005) due to
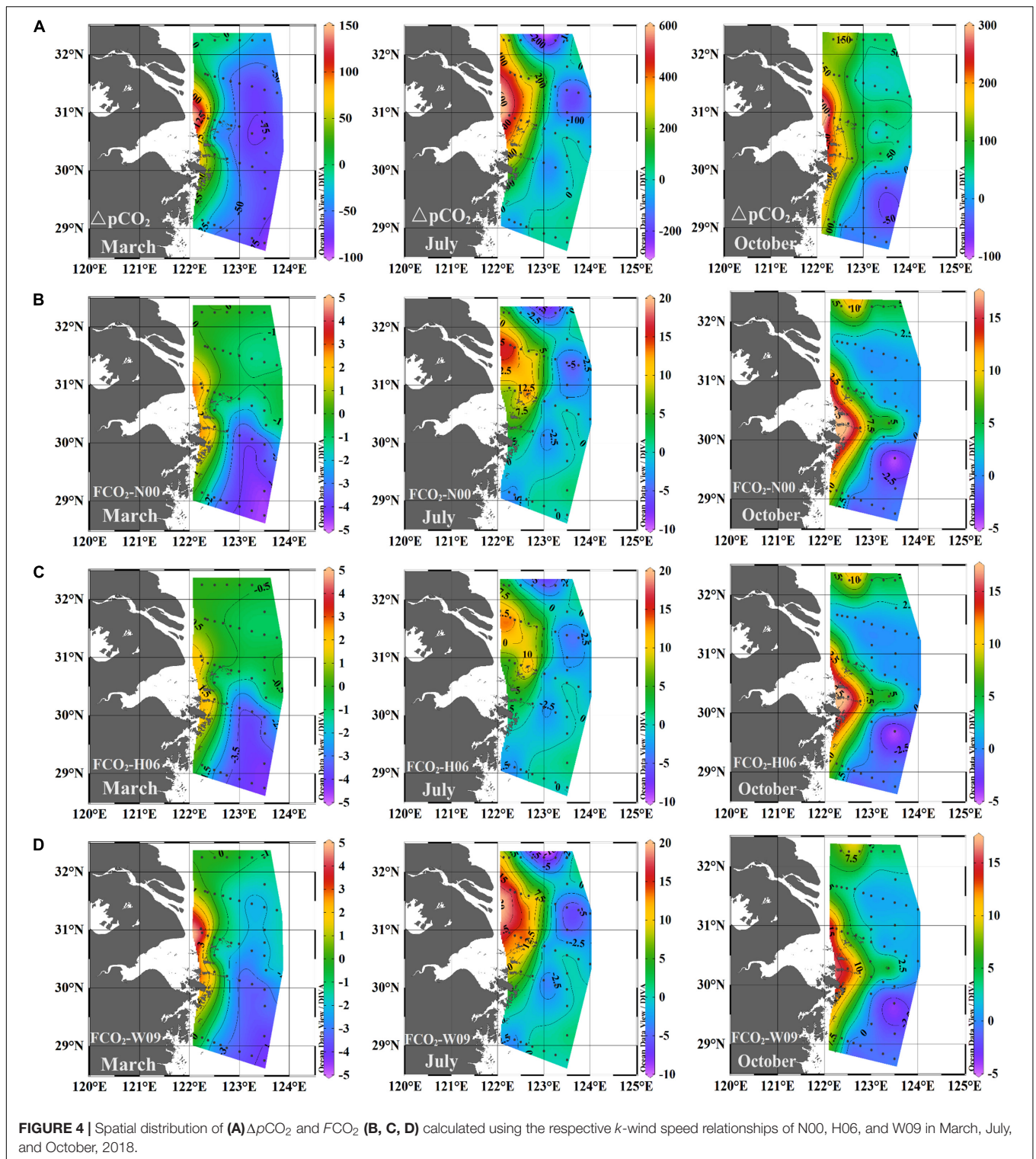
intensive carbonate weathering and erosion in the drainage basin (Zhang et al., 1990).

High concentrations of C_T were found in the YSW in March (2071–2205 µmol/kg) and October (1987–2082 µmol/kg). In July, a large C_T range was observed in the CDW (1675–2070 µmol/kg). Low concentrations of C_T were found in the ECSSW during the three surveys, with ranges of 2020–2061, 1786–1958, and 1941–2040 µmol/kg in March, July, and October, respectively (**Supplementary Figure 2E**).

Surface pCO_2 shared a similar yet inverse distribution to pH_T, (**Supplementary Figures 2C,F**). A low pH_T and high pCO_2 were observed in the CDW (357–554 and 506–719 µatm in March and October, respectively). This was caused by the biological decomposition of organic materials imported by the Changjiang River discharge, which produced a large amount of CO_2. A low pCO_2 was seen in the YSW (344–416 and 438–561 µatm in March and October, respectively), while the lowest pCO_2 was found in the ECSSW (330–369 and 350–537 µatm in March and October, respectively). However, the CDW area exhibited a very large pCO_2 range (136–965 µatm) in July.

Air–Sea CO_2 Flux

Figure 4 shows the surface distributions of ΔpCO_2 ($pCO_{2,sea}$ − $pCO_{2,air}$) and FCO_2 (calculated after N00, H06, and W09 described in Section "CO_2 flux calculations") in the three surveys. **Table 1** summarizes the FCO_2 values for each water mass and the entire study area. Overall, the distribution patterns of ΔpCO_2 and FCO_2 were consistent with pCO_2 (**Figure 4** and **Supplementary Figure 2F**), and clear seasonal variations in FCO_2 were observed. In March, the pCO_2 of the entire study area was lower than the atmospheric CO_2 concentration, while in July and October, it was the opposite (**Table 1**). However, the pCO_2 near the Changjiang River estuary was independent of the seasons, and was always higher than the atmospheric CO_2 concentration and acted as a CO_2 source (**Figure 4**). For the three water types, ΔpCO_2 < 0 in March, ΔpCO_2 > 0 in October; in July, ΔpCO_2 > 0 in the CDW and ΔpCO_2 < 0 in the ECSSW (**Table 1**).

FIGURE 4 | Spatial distribution of **(A)** ΔpCO$_2$ and FCO$_2$ **(B, C, D)** calculated using the respective k-wind speed relationships of N00, H06, and W09 in March, July, and October, 2018.

The FCO$_2$ calculated by N00, H06, and W09 showed similar spatial distributions (**Figures 4B–D**), and the FCO$_2$ values calculated for the entire study area were also similar (**Table 1**). However, for each water mass, the FCO$_2$ calculated by W09 was different from those calculated using the other two formulas, especially for the CDW and YSW. For W09, the constant term dominated at low wind speeds, and the k value calculated by W09 was much higher than the others. The wind speed was relatively low (<4 m/s), especially in spring and summer. Therefore, the FCO$_2$ calculated by W09 was much higher than that obtained

TABLE 1 | Surface water average ΔpCO_2 (μatm) and FCO_2 (mmol CO_2/m^2/day) using three different gas transfer velocity (k) formulas for the water types in March, July, and October, 2018.

Month	Water types	ΔpCO_2 [μatm]	Wind speed [m/s]	Air–sea CO_2 flux [mmol CO_2/m^2/d]			
				N00	H06	W09	Mean $\pm$ σ
March	YSW ($n = 13$)	−34 ± 27	2.53 ± 0.25	−0.62 ± 0.5	−0.47 ± 0.4	−1.04 ± 0.8	−0.71 ± 0.6
	CDW ($n = 17$)	−0.1 ± 59	3.47 ± 1.34	−0.39 ± 1.7	−0.40 ± 1.5	−0.18 ± 2.2	−0.33 ± 1.8
	ECSSW ($n = 14$)	−68 ± 11	4.23 ± 1.40	−2.95 ± 1.4	−2.66 ± 1.4	−2.98 ± 0.8	−2.86 ± 1.2
	Whole study area ($n = 44$)	−32 ± 49	3.43 ± 1.31	−1.28 ± 1.8	−1.14 ± 1.6	−1.33 ± 1.9	−1.25 ± 1.7
July	CDW ($n = 22$)	167 ± 233	3.42 ± 0.70	4.85 ± 6.9	4.06 ± 5.9	5.99 ± 8.3	4.97 ± 7.1
	ECSSW ($n = 24$)	−40 ± 63	3.84 ± 1.05	−1.27 ± 1.9	−1.08 ± 1.7	−1.47 ± 2.2	−1.28 ± 1.9
	Whole study area ($n = 46$)	59 ± 196	3.64 ± 0.92	1.65 ± 5.8	1.38 ± 5.0	2.10 ± 7.0	1.71 ± 5.9
October	YSW ($n = 16$)	76 ± 45	3.90 ± 1.85	3.38 ± 3.5	3.10 ± 3.4	3.42 ± 2.6	3.30 ± 3.1
	CDW ($n = 8$)	165 ± 64	4.72 ± 1.54	9.08 ± 5.2	8.39 ± 5.2	8.53 ± 4.0	8.67 ± 4.6
	ECSSW ($n = 26$)	29 ± 47	4.36 ± 1.68	1.21 ± 2.6	1.09 ± 2.5	1.26 ± 2.3	1.18 ± 2.5
	Whole study area ($n = 50$)	66 ± 68	4.27 ± 1.70	3.16 ± 4.3	2.90 ± 4.2	3.11 ± 3.7	3.06 ± 4.1

The values in this table are in the form of mean $\pm$ SD.

from the other two formulas (**Table 1**). Overall, the study area was a CO_2 sink in March and a CO_2 source to the atmosphere in July and October. The average FCO_2 was −1.25 ± 1.7, 1.71 ± 5.9, and 3.06 ± 4.1 mmol CO_2/m^2/day, respectively (**Table 1**). According to the average FCO_2 calculated by the three gas exchange formulas, the water type acts as a source or sink of CO_2, which may change with the seasons (**Figure 5**). The YSW and ECSSW were net CO_2 sinks in March and July (−0.71 ± 0.6 mmol CO_2/m^2/day in the YSW and −2.86 ± 1.2, −1.28 ± 1.9 mmol CO_2/m^2/day in the ECSSW) and transformed to net sources by October (3.30 ± 3.1 mmol CO_2/m^2/day in the YSW and 1.18 ± 2.5 mmol CO_2/m^2/day in the ECSSW). The CDW was a net CO_2 sink in March and a net CO_2 source in July and October (−0.33 ± 1.8, 4.97 ± 7.1, and 8.67 ± 4.6 mmol CO_2/m^2/day in March, July, and October, respectively).

Water Mixing Behavior of the Surface Water Carbonate System

A_T is considered a *quasi*-conservative carbonate parameter, and its relationship with salinity can indicate water mixing behavior (Zhai et al., 2014a,b). **Figure 6** shows that they were found significant correlations between the A_T and salinity of the three water types in March, July, and October. The lowest A_T and salinity were detected in the CDW, while the YSW had the highest A_T values.

In the YSW, there was a negative relationship between A_T and salinity in March and October [Eqs. (5) and (6), **Figures 6A,C**].

$$A_T^{YSW} = -36.41 \times Salinity + 3489.40$$
$$(\text{March}, n = 13, r = -0.727, P < 0.01) \quad (5)$$

$$A_T^{YSW} = -21.40 \times Salinity + 2928.33$$
$$(\text{October}, n = 16, r = -0.833, P < 0.01) \quad (6)$$

If Eqs. (5) and (6) were extrapolated to the average salinity of the ECSSW in March (32.80) and October (33.16), the calculated A_T values were 2295.15 and 2218.71 μmol/kg in March and

October, respectively. These values are very close to the average A_T values of the ECSSW in March and October (**Supplementary Table 1**). This result suggests water mixing between the YSW and ECSSW in March and October.

In the CDW and ECSSW, A_T–salinity had positive relationships in March, July, and October (Eqs. (7)–(12), **Figure 6**):

$$A_T^{CDW} = 6.79 \times Salinity + 2054.12$$
$$(\text{March}, n = 17, r = 0.676, P < 0.01) \quad (7)$$

$$A_T^{ECSSW} = 7.37 \times Salinity + 2018.78$$
$$(\text{March}, n = 14, r = 0.791, P < 0.01) \quad (8)$$

$$A_T^{CDW} = 12.01 \times Salinity + 1845.90$$
$$(\text{July}, n = 22, r = 0.912, P < 0.01) \quad (9)$$

$$A_T^{ECSSW} = 5.26 \times Salinity + 2057.30$$
$$(\text{July}, n = 24, r = 0.757, P < 0.01) \quad (10)$$

$$A_T^{CDW} = 14.14 \times Salinity + 1800.78$$
$$(\text{October}, n = 8, r = 0.955, P < 0.01) \quad (11)$$

$$A_T^{ECSSW} = 2.30 \times Salinity + 2162.64$$
$$(\text{October}, n = 26, r = 0.312, P = 0.12) \quad (12)$$

There was no significant correlation between the salinity and A_T in the ECSSW in October [Eq. (12)]. The Changjiang river end-member has an A_T of 1711–1831 μmol/kg in spring, 1630–1950 μmol/kg in summer (Zhai et al., 2007), and 1712–1781 μmol/kg in autumn (Xiong et al., 2019). If Eqs. (7), (9), and (11) were extrapolated to the freshwater end-member (salinity = 0), the intercept of A_T was 2054.12, 1845.90, and 1800.78 μmol/kg. The value in March is much higher than the reported A_T range (Zhai et al., 2007), possibly owing to the CDW mixing with high A_T YSW. If Eqs. (7), (9), and (11) extrapolated to the ECSSW average salinity (32.80 in March,
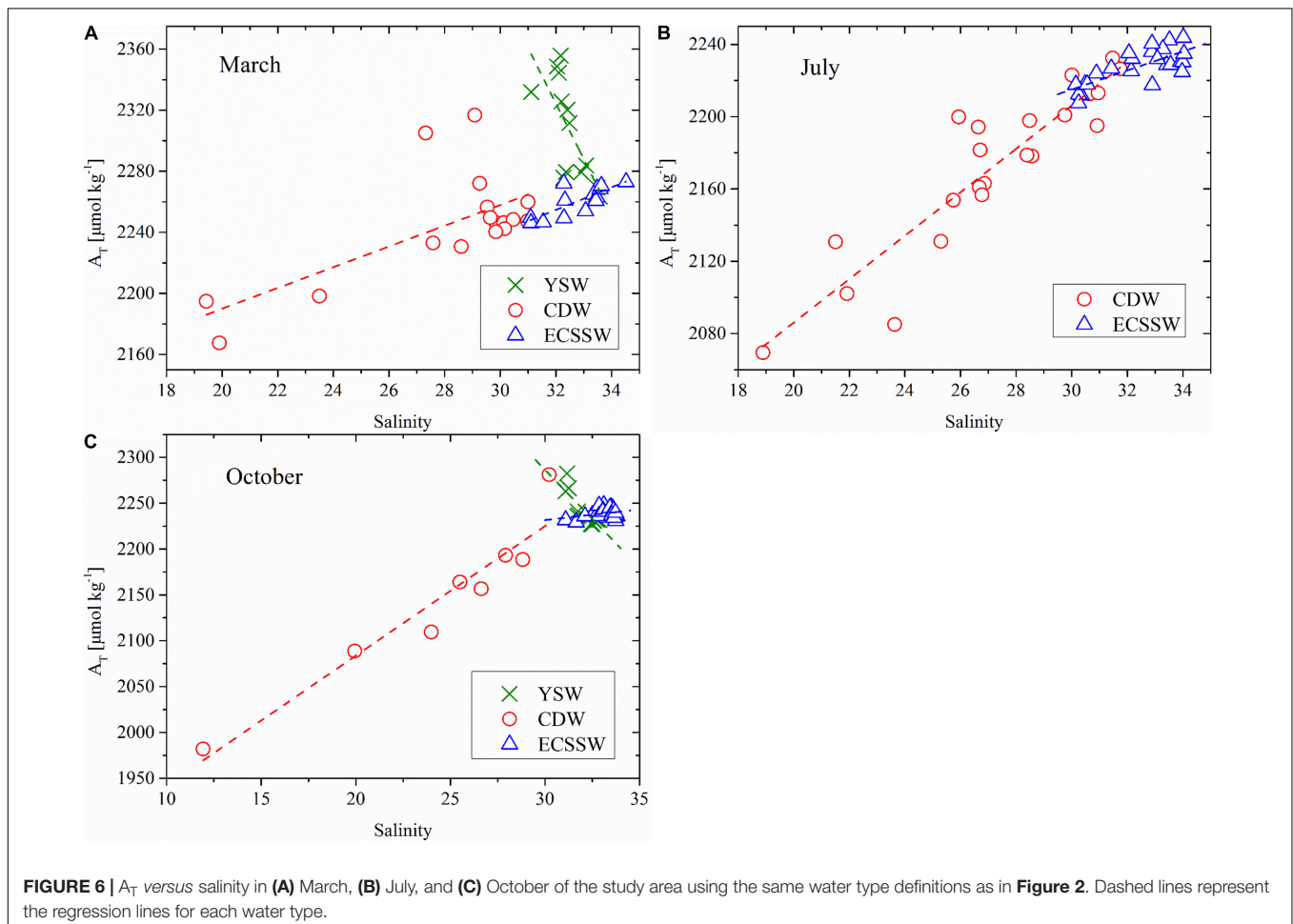
FIGURE 5 | Air–sea CO_2 fluxes in the different water types in March, July, and October, 2018. The FCO_2 in this figure were the average values calculated by the three gas exchange formulas mentioned in Section "CO_2 flux calculations."
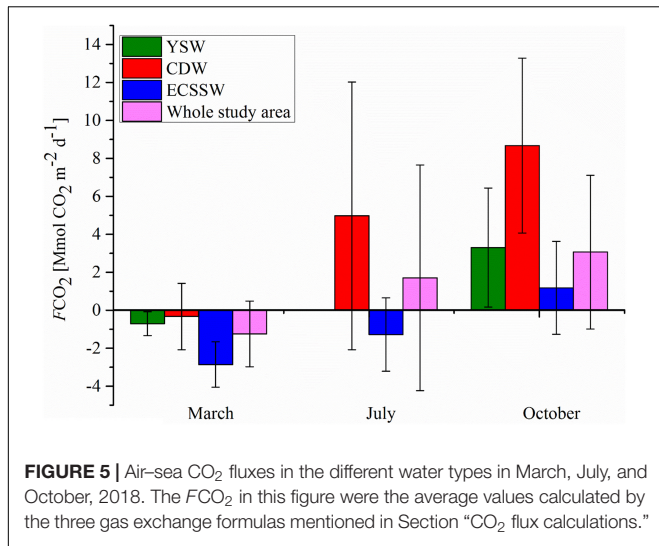
32.34 in July, and 33.16 in October), the calculated A_T results were 2276.83, 2234.30, and 2269.66 μmol/kg, respectively, which were very close to the observed average A_T values of the ECSSW (**Supplementary Table 1**). This indicates mixing between the

CDW and ECSSW during the three surveys. The A_T range of the Kuroshio (KS) and TWC surface water was 2300–2310 μmol/kg at a salinity of 35 (Chen and Wang, 1999). Extrapolating to salinity = 35, the A_T values were 2291.77, 2276.73, and 2295.68 μmol/kg using Eqs. (7), (8), and (11), respectively, which were close to the range of KS and TWC surface water. Thus, the ECS offshore end-member was dominated by TWC surface water, agreeing with the results obtained by Chen et al. (1995).

DISCUSSION

Processes Controlling the Seasonal Variation of Sea Surface Water pCO_2

Compared with the changes in the concentration of CO_2 in the atmosphere, pCO_2 varies greatly and ultimately determines the spatial and seasonal variabilities in ΔpCO_2 (Luo et al., 2015). Surface temperature and salinity-driven CO_2 solubility, water mixing, and biological processes control the temporal and spatial variabilities of sea surface pCO_2 (Wang et al., 2013). Considering the complex relationships between environmental drivers [i.e., temperature (T), salinity (S), and Chl a], and pCO_2 variation,

FIGURE 6 | A_T *versus* salinity in **(A)** March, **(B)** July, and **(C)** October of the study area using the same water type definitions as in **Figure 2**. Dashed lines represent the regression lines for each water type.

a Pearson correlation analysis was conducted to evaluate the potential drivers of pCO_2 (**Table 2**). In the following sections, the drivers shaping the pCO_2 variability in different water masses are discussed.

Relationship Between Temperature and pCO_2

Thermodynamically, pCO_2 increases exponentially with increasing temperature and follows the empirical formula of Takahashi et al. (1993):

$$\partial \ln pCO_2/\partial T = 0.0423 °C^{-1}, \tag{13}$$

Yet, pCO_2 and the temperature of the water masses in March, July, and October showed significant negative correlations (**Figures 7A–C** and **Table 2**), indicating that temperature was not the dominant factor in regulating pCO_2 variation. Similarly, a negative relationship between pCO_2 and the surface water temperature was also observed in the vertically well-mixed ECS shelf in winter (Chou et al., 2011) and the offshore area of the South Yellow Sea in winter and summer (Zhang et al., 2010). There are two major reasons for the negative relationship between pCO_2 and temperature: the first is that vertical mixing transported the CO_2-rich bottom water to the surface (Chen et al., 2007), and the second is that the intensive biological activity uptake of CO_2 dominates over the temperature effect on pCO_2 (Zhang et al., 2010) (see Section "Influences of biological processes on pCO_2 variability"). Mixing of coastal water (cold and rich in CO_2) and offshore water (warm and has lower pCO_2) is considered as the main controlling process in March and October (**Supplementary Figures 2A,F**).

Effects of Water Mixing Processes on pCO_2 Variability

To remove the influence of temperature, pCO_2 was first normalized $npCO_2 = pCO_2 \times \exp[0.0423 \times (T_{mean} - T)]$ [Eq. (13)] to the average temperatures of 11.07°C, 26.55°C, and 22.75°C in March, July, and October, respectively. **Figures 7D–F** presents the relationships between $npCO_2$ and salinity in the three different seasons. There were negative correlations between $npCO_2$ and salinity in March ($r = -0.673$, $P < 0.01$), July ($r = -0.469$, $P < 0.01$), and October ($r = -0.845$, $P < 0.01$). This suggests that pCO_2 was dominated mainly by mixing between high salinity/low pCO_2 offshore ECSSW and low salinity/high pCO_2 nearshore CDW, which is consistent with the results of Zhai and Dai (2009). Considering the relationship between $npCO_2$ and salinity in each water mass, it must be highlighted that there were strong negative correlations in

all three water masses in March and October. Furthermore, there was a significant positive correlation in the ECSSW ($r = 0.869$, $P < 0.01$) and no evident relationship in the CDW ($r = -0.171$, $P = 0.445$) in July (**Figure 7E**), which was probably caused by non-physical (i.e., metabolic) processes (Zhai and Dai, 2009).

In March, cooling resulted in the lowest pCO_2 measured in 2018, which was also shown to be a major driver of CO_2 sink (Tsunogai et al., 1999). However, the YSW and ECSSW had the highest average pCO_2 level in October (**Supplementary Table 1**) and was the atmospheric CO_2 source (**Figure 5**). The significant positive relationship between $npCO_2$ (normalized to the average temperature of 22.75°C of October) and NC_T (salinity normalized C_T, $NC_T = C_T \times 35/S$, $r = 0.939$, $P < 0.01$) (**Figure 8**) indicated that the C_T-enriched bottom water was mixed with the surface, resulting in high surface pCO_2 (Zhai and Dai, 2009; Zhang et al., 2010; Guo et al., 2015). The vertical distributions of temperature and salinity along the transects of 32°N (in the YSW) and 123°E (in the ECSSW) (**Figure 9**) indicated that deep vertical mixing occurred in October. Consequently, the YSW and ECSSW were CO_2 sources in October.

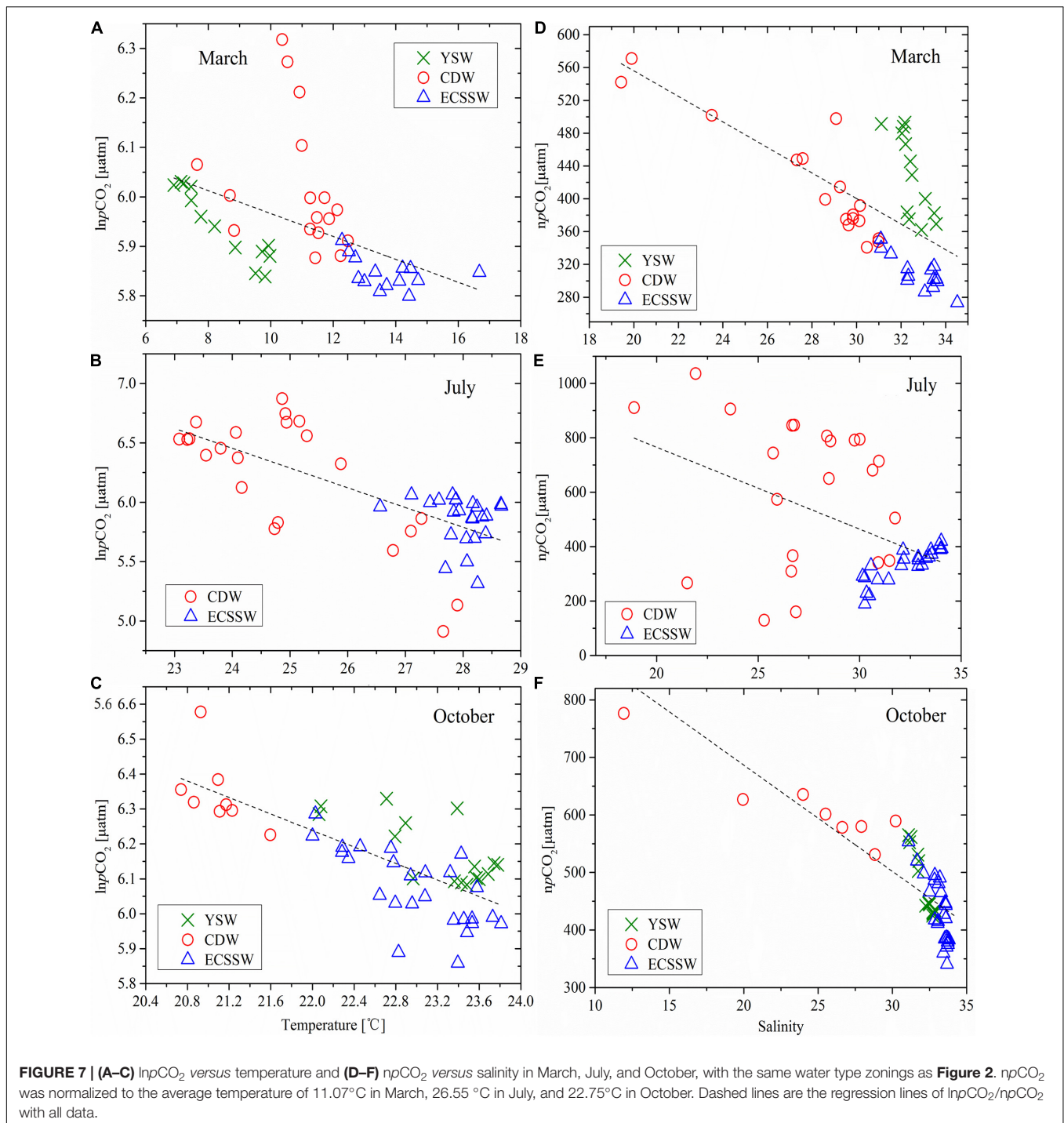## Influences of Biological Processes on pCO_2 Variability

The highest phytoplankton concentrations were found in spring and summer in the ECS, enabled by abundant nutrients and suitable temperatures (Guo et al., 2015; Qu et al., 2017). Although not an optimum indicator of biological production, the level of Chl a is often used to indicate phytoplankton biomass. During the three surveys, summer was the only season with a significant relationship between pCO_2 and Chl a (**Table 2**). The negative correlations between $npCO_2$ and Chl a in the CDW ($r = -0.675$, $P < 0.01$) and ECSSW ($r = -0.556$, $P < 0.01$) (**Figure 10**) indicated that biological production played an important role in pCO_2 drawdown. In July, phytoplankton uptake CO_2 in the surface water through photosynthesis and transport it to the deeper water through the biological pump, resulting in a corresponding decrease in surface pCO_2 and an increase in atmospheric CO_2 uptake. As a result, the ECSSW was a net CO_2 sink in July. However, the CDW acted as a CO_2 source although the biological production promoted the drawdown of surface pCO_2, which may be attributed to the Changjiang River discharge, the details were discussed in Section "Potential effects of Changjiang River discharge."

TABLE 2 | Pearson correlations of pCO_2 and potential drivers (T, S, and Chl a) in March, July, and October.

Month	March			July		October		
Water types	YSW	CDW	ECSSW	CDW	ECSSW	YSW	CDW	ECSSW
T-pCO_2	−0.943**	−0.285	−0.406	−0.671**	−0.232	−0.728**	−0.517**	−0.726**
S-pCO_2	−0.786**	−0.959**	−0.652**	−0.220	0.881**	−0.944**	−0.920**	−0.754**
Chl a-pCO_2	0.285	−0.459	−0.325	−0.686**	−0.600**	0.449	−0.115	−0.284

**Correlations (R) were statistically significant ($P < 0.01$).

FIGURE 7 | (A–C) lnpCO_2 *versus* temperature and **(D–F)** npCO_2 *versus* salinity in March, July, and October, with the same water type zonings as **Figure 2**. npCO_2 was normalized to the average temperature of 11.07°C in March, 26.55 °C in July, and 22.75°C in October. Dashed lines are the regression lines of lnpCO_2/npCO_2 with all data.
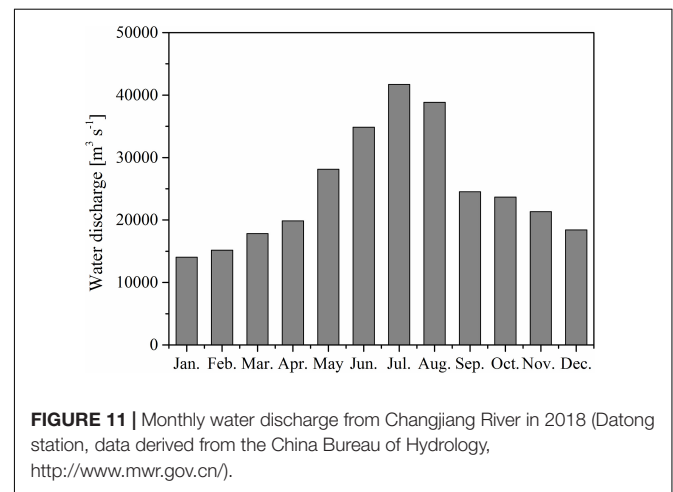
Potential Effects of Changjiang River Discharge

The CDW region is significantly affected by Changjiang River inputs (**Figure 11**) and is a major determinant of CO_2 fluxes in the ECS shelf (Tseng et al., 2011). The CO_2 sink or source status in the CDW area mainly depends on the balance of CO_2 between the contributions from the Changjiang River discharge and the consumption of biological processes (Qu et al., 2017). Here, we

adopted the method of Dai et al. (2013) to analyze why the CDW was a CO_2 source in July and October, especially in the summer, although biologically activity was high. According to Section "Water mixing behavior of the surface water carbonate system," the surface water in the CDW is a two-end member mixing between freshwater and a seawater end-member originating from the TWC surface water. **Figure 12A** shows A_T as a conservative parameter that agrees with the predicted values and confirms the
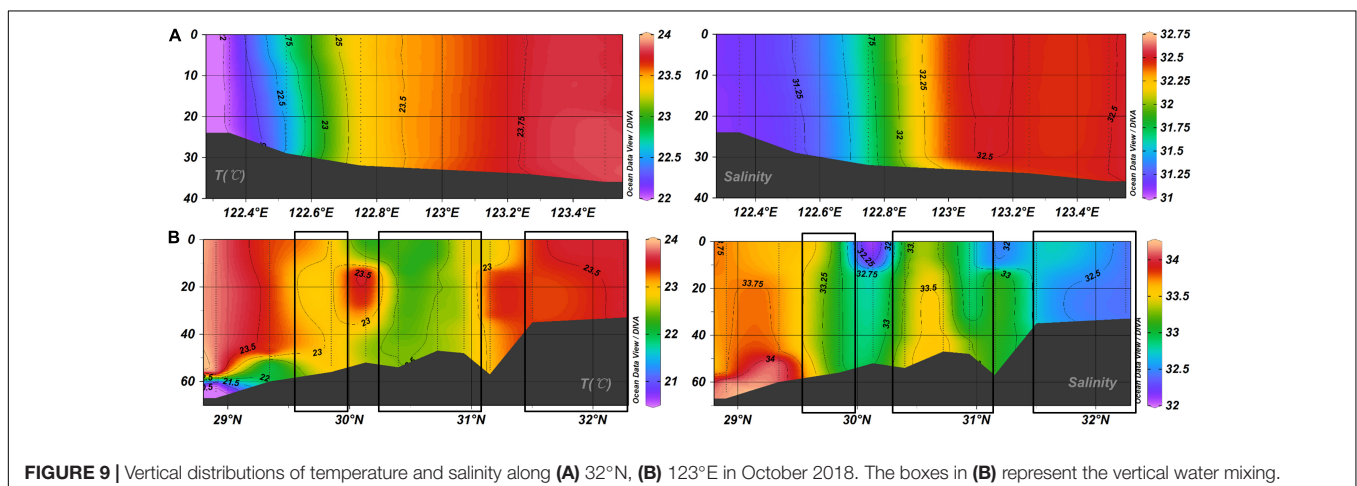
FIGURE 8 | Correlation of surface $p\text{CO}_2$ normalized to the average temperature of 22.75°C in October ($np\text{CO}_2$) and salinity normalized C_T (NC_T).

FIGURE 10 | Correlations of temperature-normalized $p\text{CO}_2$ ($np\text{CO}_2$) and Chl a of YSW and ECSSW in July. The $np\text{CO}_2$ was normalized to an average temperature of 26.55°C.
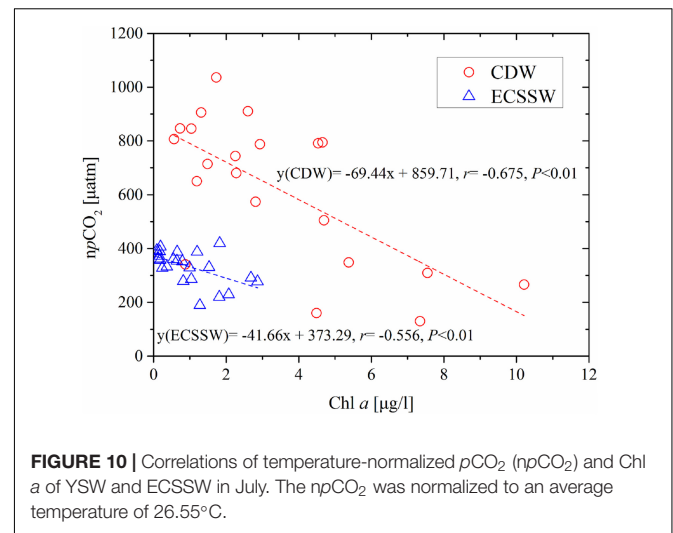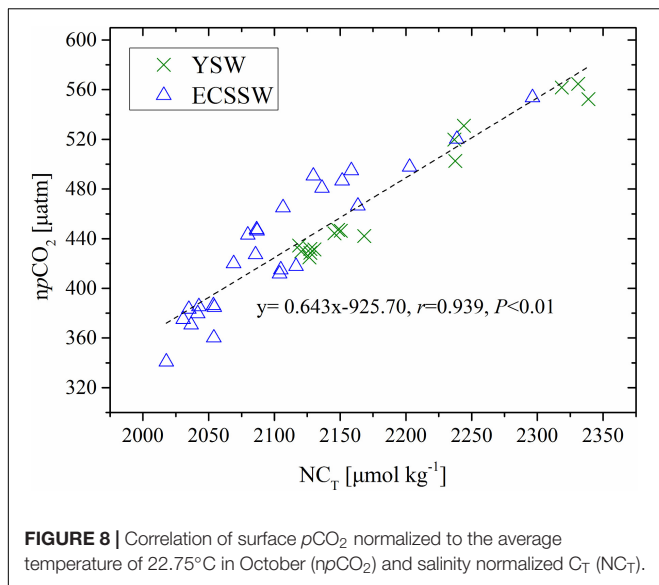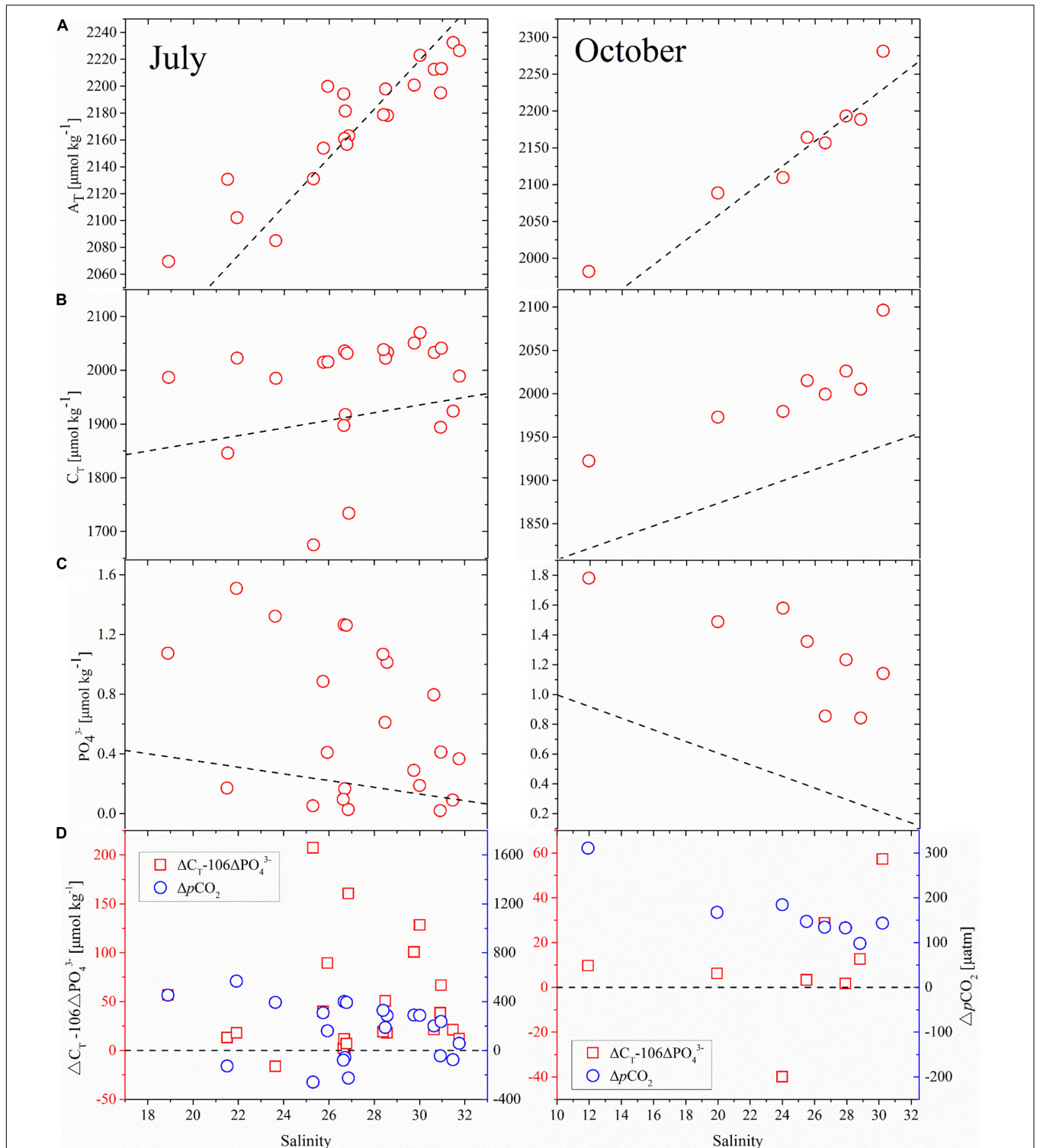
two end-members mixing in the surface water of the CDW. C_T is a non-conservative parameter that responds to biological activity. Thus, both C_T and PO_4^{3-} showed significant deviations from the predicted values (**Figures 12B,C**) below the hypothetical mixing line indicating biological removal.

Based on the method of Dai et al. (2013), ΔC_T and ΔPO_4^{3-} refer to the non-conservative portion of C_T and PO_4^{3-} in the surface water of CDW. Furthermore, the coupling of C_T and nutrient dynamics can be considered to follow the classic Redfield ratio (C: N: P = 106:16:1) (Redfield et al., 1963). When ΔC_T exceeds the corresponding $106\Delta\text{PO}_4^{3-}$, this can only be removed by CO_2 degassing into the atmosphere. In contrast, when ΔC_T is lower than the corresponding $106\Delta\text{PO}_4^{3-}$, this "deficient ΔC_T" can be compensated by atmospheric CO_2 uptake into the ocean. From **Figure 12D**, the apparent differences between ΔC_T and $106\Delta\text{PO}_4^{3-}$ were, generally, above zero; indicating extra C_T accumulation in the surface water, driving the high $p\text{CO}_2$, and for CDW to be a CO_2 source in July and October

FIGURE 11 | Monthly water discharge from Changjiang River in 2018 (Datong station, data derived from the China Bureau of Hydrology, http://www.mwr.gov.cn/).

(**Figure 5**). Therefore, in the CDW, the CO_2 produced by the decomposition and mineralization of terrestrial organic materials had exceeded the net CO_2 consumption of biological activities

FIGURE 9 | Vertical distributions of temperature and salinity along **(A)** 32°N, **(B)** 123°E in October 2018. The boxes in **(B)** represent the vertical water mixing.

FIGURE 12 | **(A)** A_T, **(B)** C_T, **(C)** PO_4^{3-}, and **(D)** $\Delta C_T - 106\Delta PO_4^{3-}$ (red squares) and ΔpCO_2 (blue circles) *versus* salinity in the surface water of CDW in July and October, 2018. The dashed lines in panels a-c represent the hypothetical mixing line between surface freshwater end-member and seawater end-member, in which A_T, C_T, and PO_4^{3-} are 1676, 1722, and 0.805 μmol/kg in July and 1724, 1744, and 1.385 μmol/kg in October in the freshwater end-member, respectively, and 2310 (Chen and Wang, 1999), 1971 (Chou et al., 2017), and 0.02 μmol/kg (Chen and Wang, 1999) in the seawater end-member, respectively. The A_T and C_T values of the freshwater end-member were obtained from Xiong et al. (2019) and the PO_4^{3-} values from station P (121.10°E, 31.75°N; **Figure 1a**), and the station samples were collected aboard the R/V *Chuangxin 2* on July 17 and October 16, 2018. The dashed line in panel d represents the pCO_2 equilibrium between the seawater and the atmosphere.

(Chen et al., 2008). The turbidity maximum zone (TMZ) is characterized by a high suspended particulate matter (SPM) concentration (Shen et al., 2020). The CDW area is very close to the TMZ in the three surveys, and Shen et al. (2020) found that a high SPM was consistent with the moving direction of the CDW. High SPM results in high turbidity and low transparency in the CDW, which is generally not optimal for phytoplankton growth and photosynthesis (Qu et al., 2017).

Seasonality in the Air–Sea CO_2 Flux

The magnitude of FCO_2 is determined by the wind speed, T- and S-driven solubility of CO_2, and ΔpCO_2. The seasonal atmospheric CO_2 sink and source pattern are determined by ΔpCO_2, and the wind speed affects the potential strength of CO_2 absorption or release (Luo et al., 2015). A Gray relational analysis was conducted to discuss the seasonal pattern of FCO_2 in different water types and its controlling factors (**Supplementary Table 2**). For the entire study area, the most influential factor for FCO_2 was ΔpCO_2 in July and October, whereas in March, wind speed, T, S, and ΔpCO_2 had similar controls on FCO_2. However, for each of the water types, the controls on FCO_2 were more complicated. In March, the most significant controlling factor of FCO_2 was ΔpCO_2 in the YSW. ΔpCO_2 was the least influential factor in the CDW and the ECSSW. In July, the most significant control on FCO_2 was ΔpCO_2 in both CDW and ECSSW. In October, wind speed was the most significant determinant of FCO_2 in the YSW and the CDW, and the most influential factor in the ECSSW was ΔpCO_2.

In March, all water types became a CO_2 sink (**Figure 5**). The average ΔpCO_2 value in ECSSW was twice that in YSW, while the average FCO_2 in ECSSW was four times that in YSW, which may be attributed to the greater wind speed (**Table 1**). Compared to the ECSSW in July, the average ΔpCO_2 (absolute value) and average wind speed were higher in March. Thus, the ECSSW was a large CO_2 sink in March (**Figure 5**). In October, the CDW was the greatest CO_2 source among the three water types as it had the highest average ΔpCO_2 value and wind speed. The CDW average ΔpCO_2 value in October was similar to that in July, but the average FCO_2 value in October was almost twice that in July due to the high wind speed (**Table 1**).

The study area, in its entirety, was a CO_2 sink in March and a source in July and October (–1.25 ± 1.7, 1.71 ± 5.9, and 3.06 ± 4.1 mmol CO_2/m^2/day, respectively) (**Figure 5** and **Table 1**). Our study in spring and autumn agreed with the findings of Zhai and Dai (2009) who found fluxes of –8.8 ± 5.8 and 2.9 ± 2.5 mmol CO_2/m^2/day, respectively. However, the Changjiang estuary was a source of CO_2 in summer (1.71 ± 5.9 mmol CO_2/m^2/day) and not a sink as shown by Zhai and Dai (2009) who reported a flux of –4.9 ± 4.0 mmol CO_2/m^2/day.

The CDW was a CO_2 sink in spring with an average FCO_2 of –0.33 ± 1.8 mmol CO_2/m^2/day, consistent with Deng et al. (2021) (–3.62 ± 7.94 mmol CO_2/m^2/day). It turned to be a CO_2 source in July with an average FCO_2 of 4.97 ± 7.1 mmol CO_2/m^2/day, consistent with Qu et al. (2017) (13.6 mmol CO_2/m^2/day). The ECSSW was a CO_2 sink in spring and summer with average FCO_2 of –2.86 ± 1.2 and –1.28 ± 1.9 mmol CO_2/m^2/day, respectively. This agrees with Qu et al. (2017) (–9.2 mmol CO_2/m^2/day in

summer) and Deng et al. (2021) (–5.53 ± 3.13 mmol CO_2/m^2/day in spring). However, the FCO_2 was calculated by a large suite of k–wind speed relationships in the above studies, which challenge a thorough comparison.

Compared to the air–sea CO_2 flux of other estuarine plumes worldwide, the FCO_2 in the Changjiang River plume was at an intermediate level and acted as a weak CO_2 source (Cai et al., 2021). The estuarine plume was a CO_2 source or sink that was not uniform (**Supplementary Table 3**). However, an estuarine plume was a CO_2 source or sink that usually varies with the season, such as Scheldt estuarine plume (Borges et al., 2008), Loire plume (Bozec et al., 2012), Pearl River plume (Zhai et al., 2013), and Changjiang River plume. Furthermore, the estimations of the magnitude and direction of air–sea CO_2 flux in estuarine plumes are influenced by the location of sampling site, the uncertainty of pCO_2, and the selected parameterization formula for the gas transfer velocity.

CONCLUSION

We investigated the surface spatial distribution and seasonal variations of pCO_2, and FCO_2 in the outer Changjiang estuary. The surface waters in the outer Changjiang estuary were grouped into three different types: YSW, CDW, and ECSSW. Seasonal variations in surface pCO_2 and FCO_2, and their major controlling factors were discussed based on various water types. The region was a net CO_2 sink in March and a net CO_2 source in July and October with an average FCO_2 of –1.25, 1.71, and 3.06 mmol CO_2/m^2/day, respectively. By March, cooling had decreased pCO_2 and led to all three water types acting as a sink for atmospheric CO_2 (–0.71, –0.33, and –2.86 mmol CO_2/m^2/day in the YSW, CDW, and ECSSW, respectively). In October, vertical mixing resulted in increased pCO_2 and the YSW and ECSSW turned to be a source of CO_2 (3.3 and 1.18 mmol CO_2/m^2/day, respectively). In July, biological CO_2 uptake had decreased pCO_2 and caused the ECSSW to be a CO_2 sink (–1.28 mmol CO_2/m^2/day). The CDW had high pCO_2 and was a CO_2 source in July and October (4.97 and 8.67 mmol CO_2/m^2/day, respectively) resulting from mineralization of terrestrial organic and inorganic materials input from the Changjiang River discharge. The high wind speeds in October further enhanced the CO_2 efflux.

The CO_2 flux regional characteristics were shown to be, generally, consistent with previous studies. However, our study showed for the first time that the outer Changjiang estuary area was a summertime source of CO_2. To further improve, and understand, air–sea CO_2 fluxes in the region, high-frequency and long-term observations of pCO_2 and supporting carbonate chemistry in the outer Changjiang estuary are required.

DATA AVAILABILITY STATEMENT

The datasets presented in this study can be found in online repositories. The names of the repository/repositories and access number(s) can be found in the article/**Supplementary Material**.

AUTHOR CONTRIBUTIONS

FUNDING

ACKNOWLEDGMENTS

SUPPLEMENTARY MATERIAL

The Supplementary Material for this article can be found online at: https://www.frontiersin.org/articles/10.3389/fmars. 2021.765564/full#supplementary-material

REFERENCES

Bauer, J. E., Cai, W. J., Raymond, P. A., Bianchi, T. S., Hopkinson, C. S., and Regnier, P. A. G. (2013). The changing carbon cycle of the coastal ocean. *Nature* 504, 61–70. doi: 10.1038/nature12857

Borges, A. V., Delille, B., and Frankignoulle, M. (2005). Budgeting sinks and sources of CO_2 in the coastal ocean: diversity of ecosystems counts. *Geophys. Res. Lett.* 32:L14601. doi: 10.1029/2005GL023053

Borges, A. V., Ruddick, K., Schiettecatte, L. S., and Delille, B. (2008). Net ecosystem production and carbon dioxide fluxes in the Scheldt estuarine plume. *BMC Ecol.* 8:15. doi: 10.1186/1472-6785-8-15

Bozec, Y., Cariou, T., Macé, E., Morin, P., Thuillier, D., and Vernet, M. (2012). Seasonal dynamics of air-sea CO_2 fluxes in the inner and outer Loire estuary (NW Europe). *Estuar. Coast. Shelf Sci.* 100, 58–71. doi: 10.1016/j.ecss.2011.05. 015

Cai, W. J. (2011). Estuarine and coastal ocean carbon paradox: CO_2 sinks or sites of terrestrial carbon incineration? *Annu. Rev. Mar. Sci.* 3, 123–145. doi: 10.1146/annurev-marine-120709-142723

Cai, W. J., and Dai, M. H. (2004). Comment on "Enhanced open ocean storage of CO_2 from shelf sea pumping". *Science* 306:1477. doi: 10.1126/science.1102132

Cai, W. J., Feely, R. A., Testa, J. M., Li, M., Evans, W., Alin, S. R., et al. (2021). Natural and anthropogenic drivers of acidification in large estuaries. *Annu. Rev. Mar. Sci.* 13, 23–55. doi: 10.1146/annurev-marine-010419011004

Cao, Z. M., Dai, M. H., Zheng, N., Wang, D. L., Li, Q., Zhai, W. D., et al. (2011). Dynamics of the carbonate system in a large continental shelf system under the influence of both a river plume and coastal upwelling. *J. Geophys. Res.* 116:G02010. doi: 10.1029/2010JG001596

Chang, P. H., and Isobe, A. (2003). A numerical study on the Changjiang diluted water in the Yellow and East China Seas. *J. Geophys. Res.* 108:3299. doi: 10.1029/ 2002JC001749

Chen, C. T. A. (2009). Chemical and physical fronts in the Bohai, Yellow and East China seas. *J. Mar. Sys.* 78, 394–410. doi: 10.1016/j.jmarsys.2008.11.016

Chen, C. T. A., and Borges, A. V. (2009). Reconciling opposing views on carbon cycling in the coastal ocean: continental shelves as sinks and near-shore ecosystems as sources of atmospheric CO_2. *Deep Sea Res. Ï.* 56, 578–590. doi: 10.1016/j.dsr2.2009.01.001

Chen, C. T. A., and Wang, S. L. (1999). Carbon, alkalinity and nutrient budgets on the East China Sea continental shelf. *J. Geophys. Res.* 104, 20675–20686. doi: 10.1029/1999JC900055

Chen, C. T. A., Huang, T. H., Chen, Y. C., Bai, Y., and Kang, Y. (2013). Air–sea exchanges of CO_2 in the world's coastal seas. *Biogeosciences* 10, 6509–6544. doi: 10.5194/bg-10-6509-2013

Chen, C. T. A., Ruo, R., Pai, S. C., Liu, C. T., and Wong, G. T. F. (1995). Exchange of water masses between the East China Sea and the Kuroshio off northeastern Taiwan. *Cont. Shelf Res.* 15, 19–39. doi: 10.1016/0278-4343(93)E0001-O

Chen, C. T. A., Zhai, W. D., and Dai, M. H. (2008). Riverine input and air-sea CO_2 exchanges near the Changjiang (Yangtze River) Estuary: status quo and implication on possible future changes in metabolic status. *Cont. Shelf Res.* 28, 1476–1482. doi: 10.1016/j.csr.2007.10.013

Chen, F. Z., Cai, W. J., Benitez-Nelson, C., and Wang, Y. C. (2007). Sea surface pCO_2–SST relationships across a cold-core cyclonic eddy: implications for understanding regional variability and air–sea gas exchange. *Geophys. Res. Lett.* 34:L10603. doi: 10.1029/2006GL028058

Chen, J. S., Wang, F. Y., Meybeck, M., He, D. W., Xia, X. H., and Zhang, L. T. (2005). Spatial and temporal analysis of water chemistry records (1958–2000) in the Huanghe (Yellow River) basin. *Glob. Biogeochem. Cycles* 19:GB3016. doi: 10.1029/2004GB002325

Chou, W. C., Gong, G. C., Cai, W. J., and Tseng, C. M. (2013). Seasonality of CO_2 in coastal oceans altered by increasing anthropogenic nutrient delivery from large rivers: evidence from the Changjiang-East China Sea system. *Biogeosciences*. 10, 3889–3899. doi: 10.5194/bg-10-3889-2013

Chou, W. C., Gong, G. C., Sheu, D. D., Hung, C. C., and Tseng, T. F. (2009). Surface distributions of carbon chemistry parameters in the East China Sea in summer 2007. *J. Geophys. Res.* 114:C07026. doi: 10.1029/2008JC005128

Chou, W. C., Gong, G. C., Tseng, C. M., Sheu, D. D., Hung, C. C., Chang, L. P., et al. (2011). The carbonate system in the East China Sea in winter. *Mar. Chem.* 123, 44–55. doi: 10.1016/j.marchem.2010.09.004

Chou, W. C., Tishchenko, P. Y., Chuang, K. Y., Gong, G. C., Shkirnikova, E. M., and Tishchenko, P. P. (2017). The contrasting behaviors of CO_2 systems in river-dominated and ocean-dominated continental shelves: a case study in the East China Sea and the Peter the Great Bay of the Japan/East Sea in summer 2014. *Mar. Chem.* 195, 50–60. doi: 10.1016/j.marchem.2017.04.005

Dai, A. G., and Trenberth, K. E. (2002). Estimates of freshwater discharge from continents: latitudinal and seasonal variations. *J. Hydrometeorol.* 3, 660–685. doi: 10.1175/1525-75412002003<0660:EOFDFC>2.0.CO;2

Dai, M. H., Cao, Z. M., Guo, X. H., Zhai, W. D., Liu, Z. Y., Yin, Z. Q., et al. (2013). Why are some marginal seas sources of atmospheric CO_2? *Geophys. Res. Lett.* 40, 2154–2158. doi: 10.1002/grl.50390

Deng, X., Zhang, G. L., Xin, M., Liu, C. Y., and Cai, W. J. (2021). Carbonate chemistry variability in the southern Yellow Sea and East China Sea during spring of 2017 and summer of 2018. *Sci. Total Environ.* 779:146376. doi: 10. 1016/j.scitotenv.2021.146376

Dickson, A. G. (1990). Standard potential of the reaction: $AgCl(s) + 1/2 H_2(g) = Ag(s) + HCl(aq)$, and the standard acidity constant of the ion HSO_4^- in

synthetic sea water from 273.15 to 318.15 K. *J. Chem. Thermodyn.* 22, 113–127. doi: 10.1016/0021-9614(90)90074-Z

Dickson, A. G., and Millero, F. J. (1987). A comparison of the equilibrium constants for the dissociation constants of carbonic acid in seawater media. *Deep Sea Res. A Oceanogr. Res. Papers* 34, 1733–1743. doi: 10.1016/0198-0149(87)90021-5

Dickson, A. G., Sabine, C. L., and Christian, J. R. (2007). *Guide to Best Practices for Ocean CO_2 Measurements. PICES Spec. Publ.*, No.3. Sidney: North Pacific Marine Science Organization, 191.

Douglas, N. K., and Byrne, R. H. (2017). Achieving accurate spectrophotometric pH measurements using unpurified meta-cresol purple. *Mar. Chem.* 190, 66–72. doi: 10.1016/j.marchem.2017.02.004

Friedlingstein, P., Jones, M. W., O'Sullivan, M., Andrew, R. M., Hauck, J., Peters, G. P., et al. (2019). Global carbon budget 2019. *Earth Syst. Sci. Data* 11, 1783–1838. doi: 10.5194/essd-11-1783-2019

Gong, G. C., Chen, Y. L. L., and Liu, K. K. (1996). Chemical hydrography and chlorophyll a distribution in the East China Sea in summer: implications in nutrient dynamics. *Cont. Shelf Res.* 16, 1561–1590. doi: 10.1016/0278-4343(96)00005-2

Guo, X. H., Cai, W. J., Huang, W. J., Wang, Y. C., Chen, F. Z., Murrell, M. C., et al. (2012). Carbon dynamics and community production in the Mississippi River plume. *Limnol. Oceanogr.* 57, 1–17. doi: 10.4319/lo.2012.57.1.0001

Guo, X. H., Zhai, W. D., Dai, M. H., Zhang, C., Bai, Y., Xu, Y., et al. (2015). Air-sea CO_2 fluxes in the East China Sea based on multiple-year underway observations. *Biogeoscience* 12, 5495–5514. doi: 10.5194/bg-12-5495-2015

Hansson, I. (1973). A new set of acidity constants for carbonic acid and boric acid in sea water. *Deep Sea Res. Oceanogr.Abstracts* 20, 461–478. doi: 10.1016/0011-7471(73)90100-9

Ho, D. T., Law, C. S., Smith, M. J., Schlosser, P., Harvey, M., and Hill, P. (2006). Measurements of air-sea gas exchange at high wind speeds in the Southern Ocean: implications for global parameterizations. *Geophys. Res. Lett.* 33:L16611. doi: 10.1029/2006GL026817

Hudson-Heck, E., and Byrne, R. H. (2019). Purification and characterization of thymol blue for spectrophotometric pH measurements in rivers, estuaries, and oceans. *Anal. Chim. Acta* 1090, 91–99. doi: 10.1016/j.aca.2019.09.009

Laruelle, G. G., Dürr, H. H., Slomp, C. P., and Borges, A. V. (2010). Evaluation of sinks and sources of CO_2 in the global coastal ocean using a spatially-explicit typology of estuaries and continental shelves. *Geophys. Res. Lett.* 37:L15607. doi: 10.1029/2010GL043691

Lee, H. J., and Chao, S. Y. (2003). A climatological description of circulation in and around the East China Sea. *Deep Sea Res. Pt. II* 50, 1065–1084. doi: 10.1016/S0967-0645(03)00010-9

Lewis, E., and Wallace, D. W. R. (1998). *Program Developed for CO_2 System Calculations, ORNL/CDIAC-105.* Oak Ridge, Ten: Carbon Dioxide Information Analysis Center.

Luan, H. L., Ding, P. X., Wang, Z. B., Ge, J. Z., and Yang, S. L. (2016). Decadal morphological evolution of the Yangtze Estuary in response to river input changes and estuarine engineering projects. *Geomorphology* 265, 12–23. doi: 10.1016/j.geomorph.2016.04.022

Lueker, T. J., Dickson, A. G., and Keeling, C. D. (2000). Ocean pCO_2 calculated from dissolved inorganic carbon, alkalinity, and equations for K_1 and K_2: validation based on laboratory measurements of CO_2 in gas and seawater at equilibrium. *Mar. Chem.* 70, 105–119. doi: 10.1016/S0304-4203(00)00022-0

Luo, X. F., Wei, H., Liu, Z., and Zhao, L. (2015). Seasonal variability of air–sea CO_2 fluxes in the Yellow and East China Seas: a case study of continental shelf sea carbon cycle model. *Cont. Shelf Res.* 107, 69–78. doi: 10.1016/j.csr.2015.07.009

McKee, B. A., Aller, R. C., Allison, M. A., Bianchi, T. S., and Kineke, G. C. (2004). Transport and transformation of dissolved and particulate materials on continental margins influenced by major rivers: benthic boundary layer and seabed processes. *Cont. Shelf Res.* 24, 899–926. doi: 10.1016/j.csr.2004.02.009

Mehrbach, C., Culberson, C. H., Hawley, J. E., and Pytkowicz, R. M. (1973). Measurement of the apparent dissociation constants of carbonic acid in seawater at atmospheric pressure. *Limnol. Oceanogr.* 18, 897–907. doi: 10.4319/lo.1973.18.6.0897

Millero, F. J., Graham, T. B., Huang, F., Bustos-Serrano, H., and Pierrot, D. (2006). Dissociation constants of carbonic acid in seawater as a function of salinity and temperature. *Mar. Chem.* 100, 80–94. doi: 10.1016/j.marchem.2005.12.001

Mintrop, L., Pérez, F. F., González-Dávila, M., Santana-Casiano, J. M., and Körtzinger, A. (2000). Alkalinity determination by potentiometry:

intercalibration using three different methods. *Cien. Mar.* 26, 23–37. doi: 10.7773/cm.v26i1.573

Nightingale, P. D., Malin, G., Law, C., Watson, A. J., Liss, P. S., Liddicoat, M. I., et al. (2000). In situ evaluation of air-sea gas exchange parameterizations using novel conservative and volatile tracers. *Glob. Biogeochem. Cyc.* 14, 373–387. doi: 10.1029/1999GB900091

Parsons, T. R., Maita, Y., and Lalli, C. M. (1984). *A Manual of Chemical and Biological Methods for Seawater Analysis.* Oxford: Pergamon Press 1, 173.

Pelletier, G. J., Lewis, E., and Wallace, D. W. R. (2011). *CO2SYS.XLS: A Calculator for the CO_2 System in Seawater for Microsoft Excel/VBA, Version 16.* Olympia, WA: Washington State Department of Ecology.

Qi, J. F., Yin, B. S., Zhang, Q. L., Yang, D. Z., and Xu, Z. H. (2014). Analysis of seasonal variation of water masses in East China Sea. *Chin. J. Oceanol. Limn.* 32, 958–971. doi: 10.1007/s00343-014-3269-1

Qu, B. X., Song, J. M., Yuan, H. M., Li, X. G., Li, N., and Duan, L. Q. (2017). Comparison of carbonate parameters and air–sea CO_2 flux in the southern Yellow Sea and East China Sea during spring and summer of 2011. *J. Oceanogr.* 73, 365–382. doi: 10.1007/s10872-016-0409-6

Qu, B. X., Song, J. M., Yuan, H. M., Li, X. G., Li, N., Duan, L. Q., et al. (2015). Summer carbonate chemistry dynamics in the Southern Yellow Sea and the East China Sea: regional variations and controls. *Cont. Shelf Res.* 111, 250–261. doi: 10.1016/j.csr.2015.08.017

Redfield, A. C., Ketchum, B. H., and Feely, R. A. (1963). "The influence of organisms on the composition of seawater," in *The Sea*, ed. M. N. Hill (New York, NY: Wiley), 26–77.

Reggiani, E. R., King, A. L., Norli, M., Jaccard, P., Sørensen, K., and Bellerby, R. G. J. (2016). FerryBox-assisted monitoring of mixed layer pH in the Norwegian Coastal Current. *J. Mar. Sys.* 162, 29–36. doi: 10.1016/j.jmarsys.2016.03.017

Shen, Z., Zhou, S., and Pei, S. (2020). *Removal and Mass Balance of Phosphorus and Silica in the Turbidity Maximum Zone of the Changjiang Estuary. Springer Earth System Sciences.* Berlin: Springer.

Shim, J. H., Kim, D., Kang, Y. C., Lee, J. H., Jang, S. T., and Kim, C. H. (2007). Seasonal variations in pCO_2 and its controlling factors in surface seawater of the northern East China Sea. *Cont. Shelf Res.* 27, 2623–2636. doi: 10.1016/j.csr.2007.07.005

Takahashi, T., Olafsson, J., Goddard, J., Chipman, D. W., and Sutherland, S. C. (1993). Seasonal variation of CO_2 and nutrients in the high-latitude surface oceans: a comparative study. *Glob. Biogeochem. Cycles* 7, 843–878. doi: 10.1029/93GB02263

Tan, Y., Zhang, L. J., Wang, F., and Hu, D. X. (2004). Summer surface water pCO_2 and CO_2 flux at air – sea interface in western part of the East China Sea. *Oceanol. Limnol. Sin.* 35, 239–245.

Tseng, C. M., Liu, K. K., Gong, G. C., Shen, P. Y., and Cai, W. J. (2011). CO_2 uptake in the East China Sea relying on Changjiang runoff is prone to change. *Geophys. Res. Lett.* 38, L24609. doi: 10.1029/2011GL049774

Tsunogai, S., Watanabe, S., and Sato, T. (1999). Is there a "continental shelf pump" for the absorption of atmospheric CO_2? *Tellus B* 51, 701–712. doi: 10.1034/j.1600-0889.1999.t01-2-00010.x

Tsunogai, S., Watanabe, S., Nakamura, J., Ono, T., and Sato, T. (1997). A preliminary study of carbon system in the East China Sea. *J. Oceanogr.* 53, 9–17. doi: 10.1007/BF02700744

Wang, B. D. (2006). Cultural eutrophication in the Changjiang (Yangtze River) plume: history and perspective. *Estuar. Coastal Shelf Sci.* 69, 471–477. doi: 10.1016/j.ecss.2006.05.010

Wang, S. L., Chen, C. T. A., Hong, G. H., and Chung, C. S. (2000). Carbon dioxide and related parameters in the East China Sea. *Cont. Shelf Res.* 20, 525–544. doi: 10.1016/S0278-4343(99)00084-9

Wang, Z. A., Wanninkhof, R., Cai, W. J., Byrne, R. H., Hu, X., Peng, T. H., et al. (2013). The marine inorganic carbon system along the Gulf of Mexico and Atlantic Coasts of the United States: insights from a transregional coastal carbon study. *Limnol. Oceanogr.* 58, 325–342. doi: 10.4319/lo.2013.58.1.0325

Wanninkhof, R. (2014). Relationship between wind speed and gas exchange over the ocean revisited. *Limnol. Oceanogr. Methods* 12, 351–362. doi: 10.4319/lom.2014.12.351

Wanninkhof, R., Asher, W. E., Ho, D. T., Sweeney, C., and McGillis, W. R. (2009). Advances in quantifying air-sea gas exchange and environmental forcing. *Annu. Rev. Mar. Sci.* 1, 213–244. doi: 10.1146/annurev.marine.010908.163742

Weiss, R. F. (1974). Carbon dioxide in water and seawater: the solubility of a nonideal gas. *Mar. Chem.* 2, 203–215. doi: 10.1016/0304-4203(74)90015-2

Weiss, R. F., and Price, B. A. (1980). Nitrous oxide solubility in water and seawater. *Mar. Chem.* 8, 347–359. doi: 10.1016/0304-4203(80)90024-9

Xiong, T. Q., Liu, P. F., Zhai, W. D., Bai, Y., Liu, D., Qi, D., et al. (2019). Export flux, biogeochemical effects, and the fate of a terrestrial carbonate system: from Changjiang (Yangtze River) Estuary to the East China Sea. *Earth Space Sci.* 6:2141. doi: 10.1029/2019EA000679

Yu, P. S., Zhang, H. S., Zheng, M. H., Pan, J. M., and Bai, Y. (2013). The partial pressure of carbon dioxide and air-sea fluxes in the Changjiang River Estuary and adjacent Hangzhou Bay. *Acta Oceanol. Sin.* 32, 13–17. doi: 10.1007/s13131-013-0320-6

Zhai, W. D., and Dai, M. H. (2009). On the seasonal variation of air-sea CO_2 fluxes in the outer Changjiang (Yangtze River) Estuary, East China Sea. *Mar. Chem.* 117, 2–10. doi: 10.1016/j.marchem.2009.02.008

Zhai, W. D., Dai, M. H., and Guo, X. H. (2007). Carbonate system and CO_2 degassing fluxes in the inner estuary of Changjiang (Yangtze) River. *China. Mar. Chem.* 107, 342–356. doi: 10.1016/j.marchem.2007.02.011

Zhai, W. D., Dai, M. H., Chen, B. S., Guo, X. H., Li, Q., Shang, S. L., et al. (2013). Seasonal variations of sea–air CO_2 fluxes in the largest tropical marginal sea (South China Sea) based on multiple-year underway measurements. *Biogeosciences* 10, 7775–7791. doi: 10.5194/bg-10-7775-2013

Zhai, W. D., Chen, J. F., Jin, H. Y., Li, H. L., Liu, J. W., He, X. Q., et al. (2014a). Spring carbonate chemistry dynamics of surface waters in the northern East China Sea: water mixing, biological uptake of CO_2, and chemical buffering capacity. *J. Geophys. Res. Ocean* 119, 5638–5653. doi: 10.1002/2014JC009856

Zhai, W. D., Zheng, N., Huo, C., Xu, Y., Zhao, H. D., Li, Y. W., et al. (2014b). Subsurface pH and carbonate saturation state of aragonite on the Chinese side of the North Yellow Sea: seasonal variations and controls. *Biogeosciences* 11, 1103–1123. doi: 10.5194/bg-11-1103-2014

Zhang, G., Zhang, J., and Liu, S. (2007). Characterization of nutrients in the atmospheric wet and dry deposition observed at the two monitoring sites over Yellow Sea and East China Sea. *J. Atmos. Chem.* 57, 41–57. doi: 10.1007/s10874-007-9060-3

Zhang, J., Huang, W. W., Liu, M. G., and Zhou, Q. (1990). Drainage basin weathering and major element transport of two large Chinese rivers (Huanghe and Changjiang). *J. Geophys. Res.* 95, 277–288. doi: 10.1029/JC095iC08p13277

Zhang, L. J., Xue, L., Song, M. Q., and Jiang, C. B. (2010). Distribution of the surface partial pressure of CO_2 in the southern Yellow Sea and its controls. *Cont. Shelf Res.* 30, 293–304. doi: 10.1016/j.csr.2009.11.009

Zhu, Z. Y., Zhang, J., Wu, Y., Zhang, Y. Y., Lin, J., and Liu, S. M. (2011). Hypoxia off the Changjiang (Yangtze River) Estuary: oxygen depletion and organic matter decomposition. *Mar. Chem.* 125, 108–116. doi: 10.1016/j.marchem.2011.03.005